Oxygenation of Hydrocarbons Mediated by Mixed-Valent Basic Iron Trifluoroacetate and Valence-Separated Component Species under Gif-Type Conditions Involves Carbon- and Oxygen-Centered Radicals**

Amy E. Tapper, Jeffrey R. Long, Richard J. Staples, and Pericles Stavropoulos*

A remarkable series of iron-based systems for oxidizing hydrocarbons—such as the century-old Fenton reagent,[1] the biologically relevant Udenfriend system,[2] and the more recently developed Gif systems[3]—have received detailed attention, but the nature of the active oxidants involved (free $HO^{•}/RO^{•}$ radicals or metal-bound $Fe^{IV/V}=O/Fe^{II/III}-OO(H)$ units) and their mode of action (radical or concerted) are topics of current debate.[4, 5] Recent advances towards elucidating the functional behavior of high-valent Fe=O units, presumed to operate in biological monooxygenases (P-450,[6] sMMO[7]), have cast suspicion as to whether similar metal-centered oxidants participate in oxygenated Fenton,[4, 8] Gif,[9] and other allegedly biomimetic systems.[10] There is now consensus[11] that at least tBuOOH-dependent versions of these systems involve tBuO$^{•}$/tBuOO$^{•}$ and substrate-centered radicals (RO$^{•}$/ROO$^{•}$). The recognition that tBuOOH-supported shunt pathways of P-450-type mimics[12] frequently generate tBuO$^{•}$/tBuOO$^{•}$ radicals limits the usefulness of these systems in probing mechanistic distinctions. Evidence to support a radical mechanism[13] for mainstream H_2O_2- or O_2/Zn-dependent Gif-type systems is currently resting on insufficient experimental basis.[14] Reported in the present study is a persuasive case of a typical Gif reagent which performs oxidation of substrates with H_2O_2 in pyridine/trifluoroacetic acid (py/TFA) by radical pathways.

The reaction of $[Fe_3O(O_2CCH_3)_6(H_2O)_3]$ with excess TFA is known[15] to yield $[Fe_3O(O_2CCF_3)_6(H_2O)_3] \cdot 3.5\,H_2O$. In our hands, samples prepared in TFA/H_2O (4/1 v/v) afford red crystals of $[Fe_3O(O_2CCF_3)_6(H_2O)_3] \cdot 2.5\,H_2O \cdot CF_3COOH$ (1, see Scheme 1). The structure of 1 at 133 K (see the Supporting Information) indicates a valence-trapped state within the triangular Fe_3O core (av $Fe^{III}-O$ 1.864(8), $Fe^{II}-O$ 2.034(3) Å). Inh dimethylh sulfoxideh (DMSO),h 1G affordsh red $[Fe_3O(O_2CCF_3)_6(DMSO)_3]$ (2), whose structure at 213 K (see the Supporting Information) reveals partial valence trapping, as there is only a 0.065 Å difference between the longer and shorter Fe−O distances.

[*] Prof. P. Stavropoulos, A. E. Tapper
Department of Chemistry, Boston University
590 Commonwealth Avenue, Boston, MA 02215 (USA)
Fax: (+1) 617-353-6466
E-mail: stavro@chem.bu.edu.
Prof. J. R. Long
University of California, Berkeley, CA (USA)
Dr. R. J. Staples
Harvard University, Cambridge, MA (USA)

Supporting information for this article is available on the WWW under http://www.wiley-vch.de/home/angewandte/ or from the author.

Surprisingly, solutions of **1** or **2** in pyridine afford green [Fe^{II}(O$_2$CCF$_3$)$_2$(py)$_4$] (**3**) and red [Fe$_2^{III}$O(O$_2$CCF$_3$)$_4$(py)$_6$] · 2 py (**4**, Scheme 1). Apparently, the stronger N-donor moiety
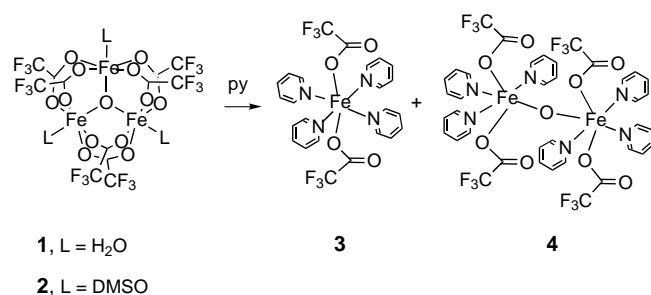
Scheme 1. Dissociation of [Fe$_3$O(O$_2$CCF$_3$)$_6$(L)$_3$] (L = H$_2$O, DMSO) in pyridine.

weakens the *trans*-oriented Fe^{II}—O ligation to cause complete dissociation of the parent Fe$_3$O core structure. Compound **3** is also obtained from a solution of [Fe(O$_2$CCF$_3$)$_2$]$_n$ in pyridine. The structure of **3** (Figure 1)[16] reveals a distorted octahedral
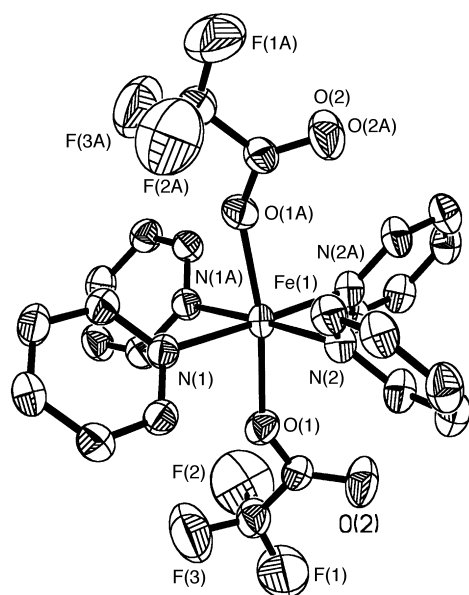

Figure 1. The structure of **3**. Selected bond lengths [Å] and angles [°]: Fe(1)–O(1) 2.069(2), Fe(1)–N(1) 2.220(3), Fe(1)–N(2) 2.205(3); O(1)-Fe(1)-O(1A) 169.90(13), N(1)-Fe(1)-N(1A) 88.95(14).

Fe environment with an imposed C_2 axis bisecting the symmetry-related N(1)-Fe(1)-N(1A) and N(2)-Fe(1)-N(2A) angles. Compound **4**, prepared independently from [Et$_4$N]$_2$-[Fe$_2$OCl$_6$] and CF$_3$CO$_2$Na, features a nearly linear μ-oxo bridge, linking two ferric sites that differ slightly in their metrical parameters (Figure 2).[16]
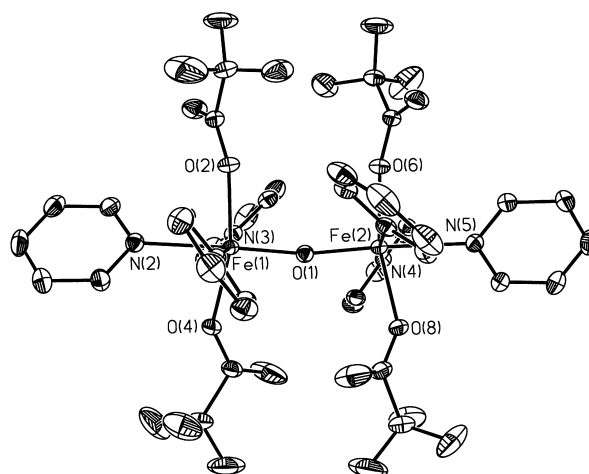

Figure 2. The structure of **4**. Selected bond lengths [Å] and angles [°]: Fe(1)–O(1) 1.7878(13), Fe(2)–O(1) 1.7854(14), Fe(1)–N(2) 2.304(2), Fe(1)–N(3) 2.160(2), Fe(1)–O(2) 2.0341(15), Fe(2)–N(5) 2.310(2), Fe(2)–N(4) 2.195(2), Fe(2)–O(6) 2.0415(15); Fe(1)-O(1)-Fe(2) 169.48(10).

Table 1 shows profiles of products derived from oxidations of the benchmark substrate adamantane (5 mmol) by the system **3** (or **4**)/H$_2$O$_2$ (0.2/2.0 mmol) in py/TFA (30.0/3.0 mL) under a stream of Ar, O$_2$ (4%) in N$_2$, or pure O$_2$. Similar results (not shown) are obtained with **1**, apparently because **1** dissociates to **3** and **4** in py/TFA. In addition to the expected oxo products, 2- and 4-adamantylpyridines are obtained not only for the *tert*-adamantyl positions (as previously recognized),[3] but also for the *sec*-adamantyl sites, especially under Ar. The presence of these coupled products provides direct evidence for the generation of *tert*- and *sec*-adamantyl radicals.[17] The reported absence of *sec*-alkylpyridines in the product profile of Gif oxygenations had led Barton and Doller[3] to propose that at least the activation of *sec* C—H bonds is brought about by nonradical pathways. Under O$_2$, the ratio of products derived due to competition between O$_2$

Table 1. Product profiles for the oxidation[a] of adamantane by H$_2$O$_2$ mediated by **3** or **4** and via authentic adamantyl radicals.[a,b]

System	Substrate								Ratio[c]
3/Ar	0.001	nd[d]	0.004	0.124	0.085	0.132	0.124		2.4
3/O$_2$ (4%)	0.003	0.016	0.117	0.120	0.077	0.018	0.018		3.5
3/O$_2$	0.034	0.027	0.143	0.128	0.078	0.001	0.001		4.2
4/Ar	0.001	0.002	0.036	0.100	0.065	0.057	0.057		3.3
4/O$_2$ (4%)	0.003	0.011	0.095	0.088	0.059	0.010	0.011		3.5
4/O$_2$	0.025	0.015	0.098	0.091	0.056	0.001	nd[d]		4.5
3/O$_2$ (4%)[b]	0.002	trace	0.027	0.029	0.032	0.002	0.003		

[a] See text for conditions. [b] By photolysis of the PTOC esters of Barton et al.[19] [c] Ratio of products (tertiary/secondary) obtained via tertiary and secondary adamantyl radicals. [d] nd = not detected.

and [pyNH]$^+$ in trapping adamantyl radicals shifts profoundly in favor of oxo species at the secondary position and to a much lesser extent at the tertiary site. Minisci et al.[18] have traced this behavior to the superior rate constant (by two orders of magnitude) and inferior reversibility for the addition reaction of *tert*-adamantyl versus *sec*-adamantyl radicals to protonated pyridine.
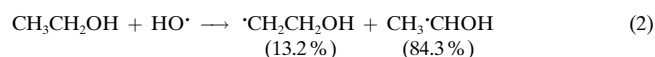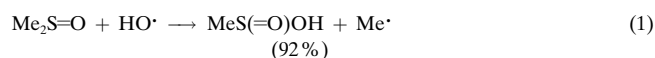
Generation of *tert*- and *sec*-adamantyl radicals in the presence of **3** by photolysis of the appropriate PTOC esters of Barton et al.[19] (Scheme 2) in py/TFA under O$_2$ (4 %) provides ratios of oxo- versus pyridine-trapped adamantyl
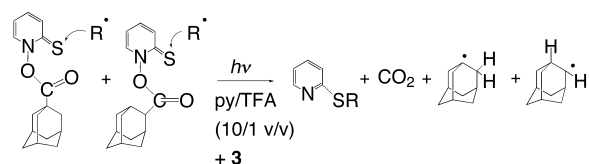
Scheme 2. Generation of authentic *tert*- and *sec*-adamantyl radicals.

products (Table 1) which for both the tertiary (0.03) and secondary positions (5.4) are comparable to those obtained by the analogous Gif experiment (*tert* 0.02, *sec* 3.7). Therefore the product profiles of adamantane oxidation are entirely dictated by the generation of *tert*- and *sec*-adamantyl radicals.

The normalized tertiary/secondary selectivities suggest that a fairly indiscriminate oxidant is involved under Ar, coupled to a more selective oxidant in the presence of O$_2$. The addition reaction of HO$^\bullet$ to DMSO [Eq. (1)] and the competitive hydrogen abstraction from EtOH [Eq. (2)] have been used[20]

$$Me_2S=O + HO^\bullet \longrightarrow MeS(=O)OH + Me^\bullet \quad (1)$$
$$(92\%)$$

$$CH_3CH_2OH + HO^\bullet \longrightarrow {}^\bullet CH_2CH_2OH + CH_3{}^\bullet CHOH \quad (2)$$
$$(13.2\%) \qquad (84.3\%)$$

to investigate the possible involvement of HO$^\bullet$, by monitoring the formation of pyridine-trapped alkyl radicals produced in these reactions under a constant stream of Ar. Table 2 reveals that the reagent **3**/H$_2$O$_2$ oxidizes DMSO/EtOH (5 mmol/ 3–10 mmol) in py/TFA (30.0/3.0 mL) as predicted by Equations (1) and (2).

Furthermore, the average k_{EtOH}/k_{DMSO} value of 0.32(4), roughly evaluated from the ratio of methylpyridines over hydroxyethylpyridines and the initial concentrations of DMSO and EtOH, is consistent with the ratio of rate constants ($k_{EtOH}/k_{DMSO} = 0.29$) reported[20] by virtue of HO$^\bullet$

attack on DMSO/EtOH in aqueous pulse radiolysis experiments. The reaction in Equation (3), which is known[21] to proceed at near diffusion controlled rates, may limit the preciseness of the assessment, further assisted by the reversibility of the addition reaction of α-hydroxyethyl radicals to [pyNH]$^+$.[17]

$$Fe^{III} + CH_3{}^\bullet CHOH \longrightarrow Fe^{II} + H^+ + CH_3CHO \quad (3)$$
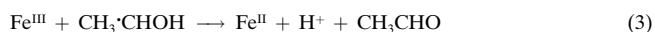
However, the total amount of iron is kept at low levels with respect to py/TFA. Most importantly, it is found that Fe^{III} sites are destabilized by the electron-withdrawing TFA (or picolinate[22]), and are rapidly reduced to Fe^{II} in the presence of stoichiometric amounts of H$_2$O$_2$, probably in conjunction with H$_2$O$_2$ dismutation. This further argues in support of a central role for the Fe^{II}/H$_2$O$_2$ combination in generating the active oxidant. In a reinterpretation of the Gif mechanism, Barton et al.[23] had accepted that the Fe^{II}/H$_2$O$_2$ "manifold" (as opposed to Fe^{III}/H$_2$O$_2$) produces substrate-based alkyl radicals, but maintained that the active oxidant is Fe^{IV}=O.

The present results provide compelling evidence that HO$^\bullet$ is the key hydrogen-abstracting oxidant under Ar, coupled to a more selective oxidant (most likely substrate-centered alkoxyl radicals: R$^\bullet$→ROO$^\bullet$→RO$^\bullet$) under increasing partial pressures of dioxygen. In conclusion, the findings of this report lend further support to the proposition[5] of a preponderant, carbon- and oxygen-centered radical pathway for mainstream Gif systems.

Experimental Section

A typical oxidation of adamantane was conducted as follows: The iron reagent (0.20 mmol) was dissolved under anaerobic conditions in pyridine (30.0 mL) and TFA (3.0 mL) followed by addition of adamantane (681 mg, 5.0 mmol). Degassed H$_2$O$_2$ (aq. 30 %, 0.28 mL, 2.0 mmol) was added slowly (6 h) using a syringe pump under a flow of specified gas. At the end of the reaction, oxalic acid (5 equiv per Fe) and PPh$_3$ (2 equiv per H$_2$O$_2$) were added followed by the internal standard (1,3,5-triisopropylbenzene). An aliquot (2 mL) was withdrawn for ether extraction and GC (SPB-1 column) or GC/MS analysis.

[1] C. Walling, *Acc. Chem. Res.* **1975**, *8*, 125–131.
[2] S. Udenfriend, C. T. Clark, J. Axelrod, B. B. Brodie, *J. Biol. Chem.* **1954**, *208*, 731–739.
[3] D. H. R. Barton, D. Doller, *Acc. Chem. Res.* **1992**, *25*, 504–512.
[4] a) P. A. MacFaul, D. D. M. Wayner, K. U. Ingold, *Acc. Chem. Res.* **1998**, *31*, 159–162; b) C. Walling, *Acc. Chem. Res.* **1998**, *31*, 155–157; c) S. Goldstein, D. Meyerstein, *Acc. Chem. Res.* **1999**, *32*, 547–550.
[5] M. J. Perkins, *Chem. Soc. Rev.* **1996**, 229–236.

Table 2. Product profiles of the oxidation of DMSO/EtOH by H$_2$O$_2$ mediated by **3** in py (30.0 mL)/TFA (3.0 mL) under Ar.

	Products [mmol]							k_{EtOH}/k_{DMSO}
	2-CH$_3$ py	3-CH$_3$ py	4-CH$_3$ py	2-CH(OH) py	4-C(OH)CH$_3$ py	2-CH$_2$OH py	4-CH$_2$OH py	
1[a]	0.198	0.026	0.099					
2[b]	0.154	0.016	0.078	0.026	0.011	0.003	0.002	0.29
3[c]	0.179	0.020	0.090	0.092	0.038	0.013	0.005	0.36
4[d]	0.118	0.016	0.059	0.080	0.029	0.009	0.004	0.32

[a] DMSO (5 mmol). [b] DMSO (5 mmol)/EtOH (3 mmol). [c] DMSO (5 mmol)/EtOH (7 mmol). [d] DMSO (5 mmol)/EtOH (10 mmol).

[6] M. Sono, M. P. Roach, E. D. Coulter, J. H. Dawson, *Chem. Rev.* **1996**, *96*, 2841 – 2887.

[7] B. J. Wallar, J. D. Lipscomb, *Chem. Rev.* **1996**, *96*, 2625 – 2657.

[8] D. T. Sawyer, A. Sobkowiak, T. Matsushita, *Acc. Chem. Res.* **1996**, *29*, 409 – 416.

[9] M. Newcomb, P. A. Simakov, S.-U. Park, *Tetrahedron Lett.* **1996**, *37*, 819 – 822.

[10] P. A. MacFaul, K. U. Ingold, D. D. M. Wayner, L. Que Jr., *J. Am. Chem. Soc.* **1997**, *119*, 10594 – 10598.

[11] a) F. Minisci, F. Fontana, S. Araneo, F. Recupero, L. Zhao, *Synlett* **1996**, 119 – 125; b) D. H. R. Barton, *Synlett* **1997**, 229 – 230.

[12] B. Meunier, *Chem. Rev.* **1992**, *92*, 1411 – 1456.

[13] M. J. Perkins, *Chem. Soc. Rev.* **1996**, 229 – 236.

[14] M. Newcomb, P. A. Simakov, S.-U. Park, *Tetrahedron Lett.* **1996**, *37*, 819 – 822.

[15] V. I. Ponomarev, O. S. Filipenko, L. O. Atovmyan, S. A. Bobkova, K. I. Turtè, *Sov. Phys. Dokl.* **1982**, *27*, 6 – 9.

[16] Crystal data for **3** (213 K) with $Mo_{K\alpha}$ radiation ($\lambda = 0.71073$ Å): orthorhombic, space group $Pccn$, $a = 16.698(5)$, $b = 9.074(2)$, $c = 16.587(4)$ Å, $V = 2513(1)$ Å^3, $Z = 4$, $R_1 = 0.0478$ for 2156 data with $I > 2\sigma(I)$, GOF (on F^2) = 1.108. For **4** (213 K): orthorhombic, space group $P2_12_12_1$, $a = 13.3830(1)$, $b = 16.4843(2)$, $c = 24.1315(2)$ Å, $V = 5323.60(8)$ Å^3, $Z = 4$, $R_1 = 0.0327$ for 9486 data with $I > 2\sigma(I)$, GOF (on F^2) = 1.055. Further details on the crystal structure investigations may be obtained from the Fachinformationszentrum Karlsruhe, 76344 Eggenstein-Leopoldshafen,h Germanyh (fax:h (+49) 7247-808-666; e-mail: crysdata@fiz-karlsruhe.de), on quoting the depository numbers CSD-411108 (**3**) and -411109 (**4**).

[17] F. Minisci, E. Vismara, F. Fontana, *Heterocycles* **1989**, *28*, 489 – 519.

[18] F. Recupero, A. Bravo, H.-R. Bjørsvik, F. Fontana, F. Minisci, M. Piredda, *J. Chem. Soc. Perkin Trans. 2* **1997**, 2399 – 2405.

[19] D. H. R. Barton, F. Halley, N. Ozbalik, M. Schmitt, E. Young, G. Balavoine, *J. Am. Chem. Soc.* **1989**, *111*, 7144 – 7149.

[20] G. V. Buxton, C. L. Greenstock, W. P. Helman, A. B. Ross, *J. Phys. Chem. Ref. Data* **1988**, *17*, 513 – 886.

[21] F. Minisci, A. Citterio, E. Vismara, *Tetrahedron* **1985**, *41*, 4157 – 4170.

[22] S. Kiani, A. Tapper, R. J. Staples, P. Stavropoulos, *J. Am. Chem. Soc.*, submitted.

[23] D. H. R. Barton, B. Hu, D. K. Taylor, R. U. Rojas Wahl, *J. Chem. Soc. Perkin Trans. 2* **1996**, 1031 – 1041.